Analyst

PAPER

Cite this: *Analyst*, 2015, **140**, 6676

Glutathione-stabilized palladium nanozyme for colorimetric assay of silver(I) ions†

Yan Fu, Haixiang Zhang, Shengdong Dai, Xing Zhi, Jinli Zhang and Wei Li*

Received 2nd June 2015,
Accepted 1st August 2015

DOI: 10.1039/c5an01103e

www.rsc.org/analyst

Glutathione-capped Pd nanoparticles with a size of 1.4–3.5 nm are facilely synthesized for peroxidase nanomimetics. The molar ratio of [Na_2PdCl_4]/[GSH] greatly affects the physicochemical properties including particle sizes, surface charge states and enzymatic activities. The most efficient Pd-based nanozyme, consisting of approximately 57% metallic Pd^0 species with an average diameter of 2.6 nm, exhibits the K_m value of 0.068 mM toward 3,3′,5,5′-tetramethylbenzidine and 156 mM toward hydrogen peroxide. Ag^+ selectively binds to Pd^0 species through metallophilic interactions and induces an apparent aggregation of Pd nanoparticles. This is the first report that Ag^+ significantly inhibits the peroxidase mimicking activity of Pd nanoparticles. A Pd-based nanozyme is employed to explore colorimetric detection of Ag^+ with the limit of detection of 1.2 nM. This developed sensing system is potentially applicable for quantitative detection of Ag^+ in drinking water as well as Ag nanoparticles in aqueous solution.

1. Introduction

Silver salts and silver compounds have been extensively utilized in batteries catalysts, photography, the semiconductor industry and biomedical field. Owing to antibacterial abilities, silver-based salts and nanoparticles have been employed in the disinfection of drinking water and in the production of medical materials such as bandages, prostheses and catheters.[1] Silver from industrial wastes and emissions reaches up to approximately 2500 tons annually, and about 80 tons are released to the surface water.[2] Ag^+ is liable to coordinate with amine, imidazole, carboxylate and thiol groups of proteins, resulting in their biological toxicity.[3,4] Therefore, the U.S. Environmental Protection Agency reported that Ag^+ causes toxicity to fish and microorganisms at a concentration higher than 1.6 nM, and has defined the maximum permissible limit of 0.9 μM in drinking water.

Developing fluorescent and colorimetric Ag^+-sensing systems, based on the selective interactions of Ag^+ with organic molecules,[5,6] nucleic acids,[7,8] and metal nanoclusters,[9] has shown the advantage of portable monitoring with no need of sophisticated techniques such as atomic absorption spectrometry,[10] inductively coupled plasma-atomic emission spectrometry,[11] and voltammetry.[12] For instance, Sung *et al.* developed a colorimetric Ag^+ detection method by using *N*-1-(2-mercaptoethyl)adenine functionalized gold nanoparticles (MEA-AuNPs), resulting in the limit of detection (LOD) of 3.3 nM. In this sensing system, addition of Ag^+ causes significant aggregation of MEA-AuNPs, yielding a color change from red to blue.[13] Thus, we are inspired to develop colorimetric detection of Ag^+ that produces high sensitivity and selectivity.

Palladium nanomaterials have been recognized as a kind of highly desirable catalysts, of which their catalytic activities are greatly associated with surface geometric effects, electronic properties and quantum size effects.[14] So far, water-soluble Pd nanocatalysts with excellent stabilities and desirable sizes have been successfully synthesized by using nucleation templates such as polymers, dendrimers, peptides, proteins and nucleic acids.[15–21] Recently, Pd nanoparticles or Pd-based hybrid nanostructures have been demonstrated to possess intrinsic peroxidase mimicking activities, which have been successfully used in colorimetric assays for Fe(II),[22] hydrogen peroxide,[23] glucose,[24] xanthine,[25] sarcosine,[26] prostate-specific antigen,[27] *etc*. Importantly, the most common metallophilic interactions are observed in the d^{10} configuration including Hg^{2+}, Au^+, Ag^+, Cu^+, Pd^0 and Pt^0.[28–31] The metallophilic interactions between Hg^{2+} ($4f^{14}5d^{10}$) and Pt^0 ($4f^{14}5d^{10}$) have been employed to develop ultrasensitive detection of Hg^{2+} in aqueous solution, on the basis of Hg^{2+}-induced inhibition of peroxidase mimicking activity of Pt nanoparticles.[32–35] This inspires us to employ Pd-based nanozyme for colorimetric detection of hazardous metal ions.

Reduced glutathione (GSH, γ-Glu-Cys-Gly) has functional groups including –SH, $–NH_2$ and –COOH, which exhibit high affinities to transition metal ions. Therefore, GSH has been

Key Laboratory for Green Chemical Technology MOE, Tianjin University; Collaborative Innovation Center of Chemical Science and Chemical Engineering (Tianjin), Tianjin 300072, People's Republic of China. E-mail: liwei@tju.edu.cn; Fax: +86-22-27890643; Tel: +86-22-27890643

†Electronic supplementary information (ESI) available. See DOI: 10.1039/c5an01103e

This journal is © The Royal Society of Chemistry 2015

reported to be successfully used as a stabilizing agent for the environmentally benign synthesis of noble metal nanoparticles with desirable physicochemical properties.[36–39] Moreover, the whole synthesis process of metal nanoparticles using GSH as the capping agent is eco-friendly, with little consumption of chemical reagents. Owing to the relatively low molecular weight of GSH molecules, other metal ions can easily interact with the metal surfaces of GSH-capped nanoparticles. In this paper, GSH was chosen as a nucleation template to synthesize Pd-based peroxidase nanomimetics. By using characterization of enzyme kinetics, TEM and XPS, it is demonstrated that the peroxidase-like activity of Pd-based nanozyme is greatly associated with the proportion of metallic Pd atoms. This is the first report that Ag^+ inhibits the peroxidase-like activity of Pd-based nanozyme, totally opposite to the effect of Hg^{2+} on the enzymatic activity. GSH-Pd is employed to explore colorimetric detection of Ag^+ and Ag nanoparticles in aqueous solution with high sensitivity.

2. Experimental section

2.1 Chemicals

Reduced GSH was purchased from J&K Scientific. Na_2PdCl_4 (99.9%), $CuCl_2{\cdot}2H_2O$, $Pb(CH_3COO)_2{\cdot}3H_2O$, $Hg(ClO_4)_2{\cdot}3H_2O$ and H_2O_2 (30 wt%) were purchased from Alfa Aesar. 3,3′,5,5′-Tetramethylbenzidine (TMB) was purchased from Heowns. Dimethylamine borane (DMAB) was purchased from Sigma-Aldrich. Fetal bovine serum was purchased from Lanzhou Bailing Biotechnology. Other reagents such as $AgNO_3$, Na_2HPO_4, NaH_2PO_4, NaCl, $MgCl_2{\cdot}6H_2O$, $MnCl_2{\cdot}4H_2O$, $CdCl_2{\cdot}5/2H_2O$, $ZnCl_2$, $FeCl_3{\cdot}6H_2O$, $CoCl_2{\cdot}6H_2O$, and $Ni(NO_3)_2{\cdot}6H_2O$ were purchased from Tianjin Kermel Chemical Reagent Company.

2.2 Synthesis of GSH-Pd nanoparticles

Pd nanoparticles were synthesized through the reduction of Na_2PdCl_4 by DMAB. Firstly, different concentrations of GSH (2, 5, 6.75, 12.5, 25, 50, 100, 200 μM) dissolved in 10 mM Na_2HPO_4–NaH_2PO_4 buffer (pH 5.0) were incubated with 300 μM Na_2PdCl_4 for 2 h at 25 °C. Then freshly prepared DMAB aqueous solution was added to the above mixture to the [DMAB]/[Na_2PdCl_4] ratio of 5. GSH-Pd was prepared after 12 h-reduction at 25 °C.

2.3 Reaction kinetics

Enzyme kinetics was monitored at 652 nm at 20 °C. In the reaction system, the concentration of TMB and H_2O_2 was fixed at 0.125 mM and 125 mM respectively, in NaH_2PO_4–H_3PO_4 buffer (pH 4.0). Then the as-prepared GSH-Pd was added into the above solution to a final concentration of 900 nM (calculated from the precursor). All the experiments were repeated thrice. The initial velocities (v) were calculated according to eqn (1) and (2):

$$C_p = \frac{A_{652}}{\varepsilon L} \tag{1}$$

$$v = \frac{dC_p}{dt} \tag{2}$$

where C_p is the concentration of oxTMB, ε is the extinction coefficient of oxTMB, and L is the optical path length of 1 cm.

In order to calculate the kinetic parameters of GSH-Pd, a series of solutions were prepared at various concentrations of TMB or H_2O_2. The kinetic parameters were calculated using the Michaelis–Menten eqn (3):

$$v = \frac{V_{max}[S]}{K_m + [S]} \tag{3}$$

where v is the initial velocity of the reaction, V_{max} is the maximal velocity of reaction, [S] is the substrate concentration, and K_m is the Michaelis–Menten constant.

K_m and V_{max} were fitted by using a Lineweaver–Burk plot according to eqn (4):

$$\frac{1}{v} = \frac{K_m}{V_{max}[S]} + \frac{1}{V_{max}} \tag{4}$$

2.4 Colorimetric detection of Ag^+ in aqueous solution

The sensing system contains 0.125 mM TMB, 125 mM H_2O_2, 900 nM GSH-Pd (calculated from the precursor) and different concentrations of Ag^+. Firstly, 9 μL GSH-Pd solution (precursor concentration of 300 μM) was added into 1.5 mL NaH_2PO_4–H_3PO_4 buffer (pH 4.0). After adding certain volume of $AgNO_3$ stock solution, the mixtures were diluted to 2.93 mL using triple distilled water. Finally, 15 μL of TMB stock solution (25 mM dissolved in ethanol) and 38.5 μL of H_2O_2 stock solution (30 wt% aqueous solution) were added. The A_{652} was recorded after 10 min-reaction at 25 °C. The LOD defined as 3σ/slope was calculated from the standard deviation of the blank (σ) and the slope in the linear region.

To investigate the effects of other metal ions including Na^+, Mg^{2+}, Cu^{2+}, Pb^{2+}, Cd^{2+}, Zn^{2+}, Ni^{2+}, Mn^{2+}, Fe^{3+}, Co^{2+}, and Hg^{2+}, respectively, 9 μL GSH-Pd solution was added into 1.5 mL NaH_2PO_4–H_3PO_4 buffer (pH 4.0). After adding certain volume of stock solution of different metal ions, the mixtures were diluted to 2.93 mL using triple distilled water. Finally, 15 μL of TMB stock solution (25 mM dissolved in ethanol) and 38.5 μL of H_2O_2 stock solution (30 wt% aqueous solution) were added. The A_{652} was recorded after 10 min-reaction at 25 °C.

2.5 Detection of Ag^+ in real samples

We carried out the spiked-recovery experiments and ICP-MS using the lake water collected from Jingyi Lake, Tianjin Medical University. In the sensing system, the lake water was filtered with a pore size of 0.2 μm and diluted 30-times to reach an appropriate concentration of Ag^+. The detection system was spiked with 20, 50 and 80 nM Ag^+, respectively. The detection was performed in a 3 mL-system. Firstly, certain volume of $AgNO_3$ stock solution was mixed with 100 μL pretreated water samples. Then the above mixtures were diluted to 2.93 mL by using NaH_2PO_4–H_3PO_4 buffer (pH 4.0) and triple distilled water. Finally, 9 μL GSH-Pd solution, 15 μL of

TMB stock solution (25 mM dissolved in ethanol) and 38.5 μL of H_2O_2 stock solution (30 wt% aqueous solution) were successively added. The A_{652} was recorded after 10 min-reaction at 25 °C.

2.6 Detection of Ag nanoparticles

Citrate-capped Ag nanoparticles were synthesized according to the previously reported method.[40] Firstly, different concentrations of the as-prepared Ag nanoparticles (calculated from the Ag^+ precursor) were incubated with H_2O_2 at 25 °C for 30 min, at the molar ratio of $[H_2O_2]/[Ag^+]$ of 400. Then the above mixtures were diluted to 2.93 mL by using NaH_2PO_4–H_3PO_4 buffer (pH 4.0) and triple distilled water. Finally, 9 μL GSH-Pd solution, 15 μL of TMB stock solution (25 mM dissolved in ethanol) and 38.5 μL of H_2O_2 stock solution (30 wt% aqueous solution) were successively added. The A_{652} signal was recorded after 10 min-reaction at 25 °C.

2.7 Characterization

UV-vis spectroscopy was performed on a Varian Cary300 spectrophotometer using a quartz glass cuvette with 1 cm path length. *Transmission Electron microscopy* (*TEM*) was carried out on a JEM-2010FEF equipment (JEOL, Japan). All the average sizes were obtained by measuring more than 100 dispersive nanoparticles. *X-ray Photoelectron Spectroscopy* (*XPS*) was performed on the PHI5000 Versaprobe. In the sample preparation, 30 μL of the as-prepared GSH-Pd solution was dropped onto a clean silicon wafer, and then dried under a nitrogen gas atmosphere. This process was repeated thrice. *Inductively coupled plasma mass spectrometry* (*ICPMS*) was carried out on an Agilent 7700CE to determine the concentration of Ag^+ in the lake water.

3. Results and discussion

3.1 Synthesis of GSH-capped Pd nanoparticles

GSH-capped Pd nanoparticles were prepared by using Na_2PdCl_4 as the precursor, and DMAB as the reducing agent. The physicochemical properties of GSH-Pd were investigated by varying the molar ratio of $[Na_2PdCl_4]/[GSH]$ in the synthesis process. As shown in Fig. 1a, GSH-Pd prepared at the $[Na_2PdCl_4]/[GSH]$ ratio of 3 exhibits an average diameter of 1.4 nm. The particle size gradually increases up to 3.5 nm upon increasing the $[Na_2PdCl_4]/[GSH]$ ratio from 3 to 60 (Fig. 1b and c). Therefore, we denote GSH-Pd prepared at different molar ratios of $[Na_2PdCl_4]/[GSH]$ as GSH-Pd1.4 ($[Na_2PdCl_4]/[GSH] = 3$), GSH-Pd2.6 ($[Na_2PdCl_4]/[GSH] = 6$) and GSH-Pd3.5 ($[Na_2PdCl_4]/[GSH] = 60$), respectively. In comparison, GSH-Pd nanoparticles reduced by $NaBH_4$ ($[Na_2PdCl_4]/[GSH] = 6$, $[NaBH_4]/[Na_2PdCl_4] = 2$) exhibit an average diameter of 3.8 nm (Fig. S1 in the ESI†).

As shown in Fig. 2, the deconvolution spectra of Pd 3d orbitals display two typical bands: the band at the binding energy of 336.9 eV corresponding to Pd^{2+} species and that at 334.9 eV corresponding to metallic Pd^0.[37] It is demonstrated that

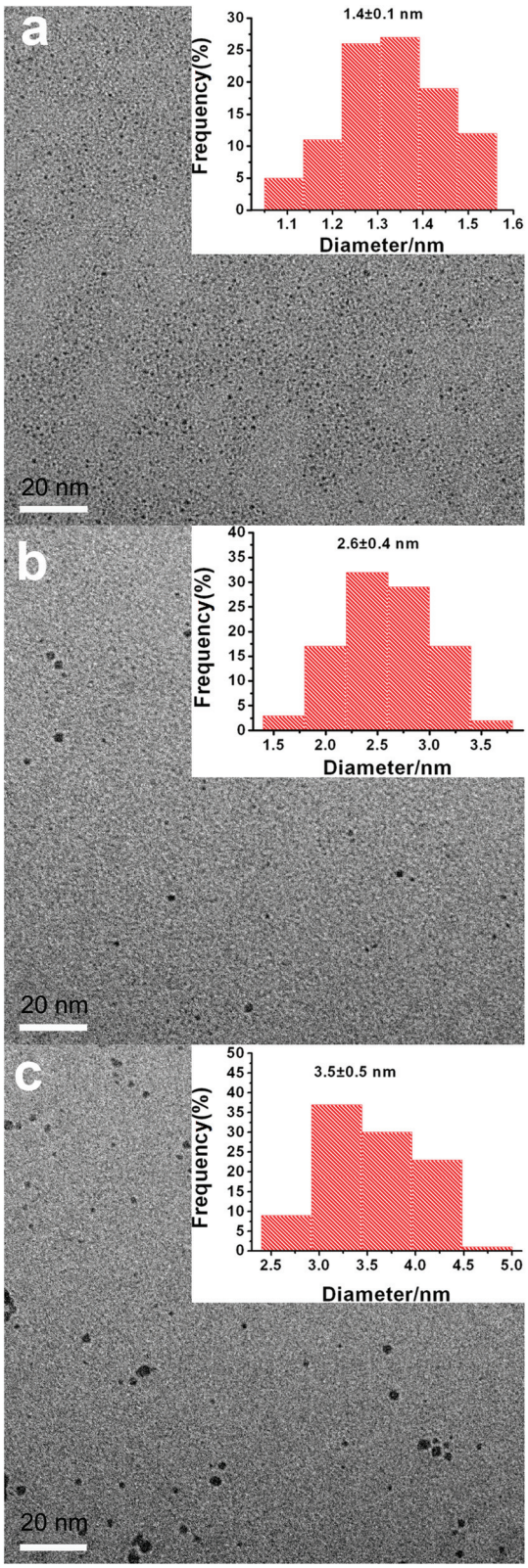

Fig. 1 TEM images of GSH-Pd reduced by DMAB ($[DMAB]/[Na_2PdCl_4] = 5$) at pH 5.0: (a) $[Na_2PdCl_4]/[GSH] = 3$, (b) $[Na_2PdCl_4]/[GSH] = 6$, (c) $[Na_2PdCl_4]/[GSH] = 60$, the scale bar is 20 nm.

 This journal is © The Royal Society of Chemistry 2015

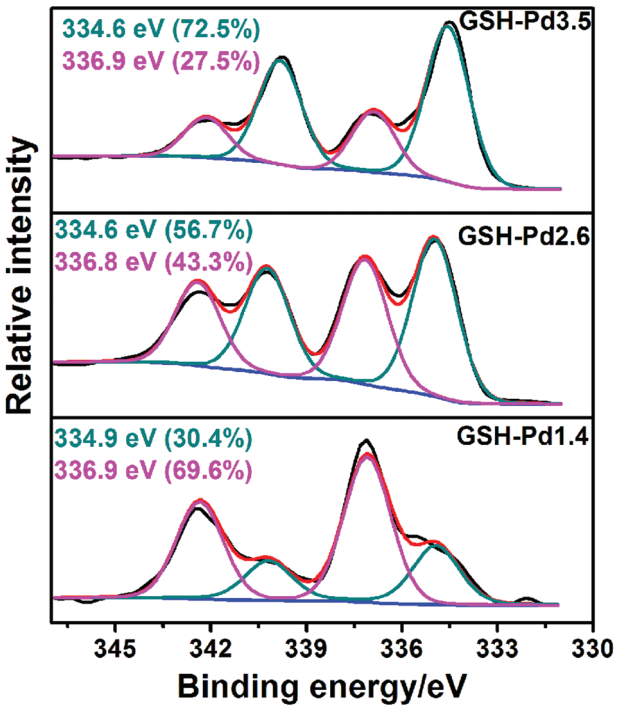

Fig. 2 Pd 3d XPS spectra of different GSH-Pd, black, red, magenta and cyan lines represent the raw, the fitted, the Pd^{2+} and the Pd^{0} components' curves, respectively.

GSH-Pd1.4 contains 70% Pd^{2+} and 30% Pd^{0} species, respectively. With the particle size increasing from 1.4 to 3.5 nm, the proportion of Pd^{0} species increases significantly from 30% to 72%, whereas the fraction of Pd^{2+} species decreases from 70% to 28%. It is demonstrated that the proportion of Pd^{2+} increases with the concentration of the GSH template. Previously, the reduction of Pt^{2+} precursors was reported to be hindered by the coordination of Pt^{2+} with amide groups of the dendrimer template.[41] Moreover, *p*-mercaptobenzoic acid-stabilized Ag nanoclusters exhibited a shell of the protecting layer through coordination between Ag and thiolate.[42] Lysozyme-stabilized Au nanoclusters was a mixture of Au^{0} and Au^{+}, of which Au^{+} species (~24%) could be assigned to Au atoms ligated with lysozyme.[43] Therefore, it is reasonable to conclude that Pd^{2+} species exist on the surface of the particles through the ligation with GSH templates.

3.2 GSH-Pd nanoparticles for peroxidase mimetics

For testing the peroxidase-like activities of GSH-Pd, steady-state kinetics was performed adopting the oxidation reaction of TMB in the presence of H_2O_2.

The initial reaction rate increases by approximately 100-times as the $[Na_2PdCl_4]$/[GSH] increases from 1.5 to 12, and then it decreases by more than 5-times as the $[Na_2PdCl_4]$/[GSH] ratio increases to 150 (Fig. S2†). Among these GSH-Pd nanoparticles, the GSH-Pd nanoparticles prepared with the $[Na_2PdCl_4]$/[GSH] ratio of 12 exhibit the highest peroxidase mimicking activity with the initial v of 0.35 μM s^{-1}.

Michaelis–Menten curves were obtained for GSH-Pd1.4, GSH-Pd2.6 and GSH-Pd3.5 respectively, by varying the concentration of TMB or H_2O_2 (Fig. 3, S3 and S4†). Upon increasing the size from 1.4 to 3.5 nm, the K_m with TMB increases from 0.045 to 0.08 mM. Oppositely, the K_m with H_2O_2 decreases from 254 to 137 mM (listed in Table 1). It is suggested that the affinity of GSH-Pd toward TMB increases with the fraction of Pd^{2+} species, whereas the affinity toward H_2O_2 increases with the proportion of metallic Pd^{0} species. GSH-Pd2.6 exhibits the highest enzymatic activity with the K_m of 0.068 mM toward TMB and 156 mM toward H_2O_2 at 20 °C, which possesses activities comparable with previously reported peroxidase nanomimetics for colorimetric detection such as Pd nanostructures, Pt nanoparticles, Au nanoclusters, Cu nanoclusters, Fe_3O_4 nanoparticles and Co_3O_4 nanotubes (as listed in Table 1). For example, Yan and coworkers reported that 30 nm Fe_3O_4 nanoparticles exhibited the K_m value of 0.098 mM toward TMB and 154 mM toward H_2O_2 at 40 °C.[44] Moreover, our previous studies have employed GSH molecules as the nucleation templates to synthesize 3.3 nm Pt nanozyme, which possessed highly peroxidase-like activity with the K_m of 0.03 mM and 88.7 mM toward TMB and H_2O_2 at 20 °C, respectively.[35] Therefore, it is demonstrated that GSH-Pd can be recognized as a promising candidate for biological detection.

3.3 Colorimetric assay of Ag^{+} in aqueous solution

To test the ability of GSH-Pd on the colorimetric detection of Ag^{+}, the sensing system contains 900 nM Pd (calculated from the precursor), 0.125 mM TMB and 125 mM H_2O_2, respectively. According to the absorption spectra of H_2O_2-mediated oxidation of TMB catalyzed GSH-Pd2.6, the absorption peak at 652 nm gradually decreases with the concentration of Ag^{+} (Fig. S5†). According to reaction kinetics, the equilibrium can be reached within 10 min in the absence or the presence of Ag^{+} (Fig. S6†). As shown in Fig. 4a, the A_{652} collected at 10 min gradually decreases with the $[Ag^{+}]$ increasing to 300 nM. The reaction rate gradually decreases with the concentration of Ag^{+}, suggesting that Ag^{+} inhibits the peroxidase-like activity of GSH-Pd (Fig. S7†). A pseudo-linear relationship can be obtained between the A_{652} and the $[Ag^{+}]$ in the concentration range of 2–100 nM, with the calibration curve of A_{652} = 1.28548–0.00725$[Ag^{+}]$. The LOD is determined to be 1.14 ± 0.003 nM from three independent experiments. In order to test the influence of Cl^{-} ions (from precursor Na_2PdCl_4) on the detection of Ag^{+}, 5 μM NaCl is additionally added into the TMB–H_2O_2 reaction system. With the concentration of 80 nM Ag^{+}, the A_{652} signal in the sensing system containing Cl^{-} is comparable to that generated in the system without Cl^{-} (Fig. S8†). Therefore, free Cl^{-} ions have a slight influence on the detection of Ag^{+}.

The selectivity of this detection method was evaluated by different interfering ions. As shown in Fig. 4b, addition of Na^{+}, Mg^{2+}, Cu^{2+}, Pb^{2+}, Cd^{2+}, Zn^{2+}, Ni^{2+}, Mn^{2+}, Fe^{3+} and Co^{2+} individually into the detection system at 10-fold concentration excess contributes to a small interference on the final A_{652}

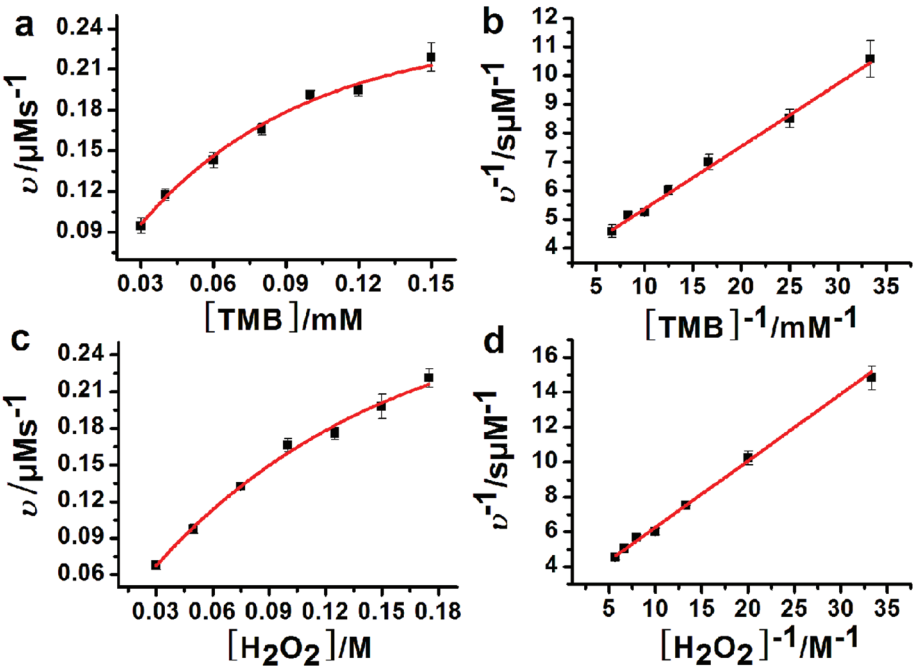

Fig. 3 Steady-state kinetics of GSH-Pd2.6 are measured through the oxidization of TMB by H_2O_2 at 20 °C using 900 nM Pd (calculated from precursor): (a) The concentration of H_2O_2 is fixed at 125 mM and the TMB concentration is varied, (c) The concentration of TMB is fixed at 0.125 mM and the H_2O_2 concentration is varied, (b) and (d) are double-reciprocal plots of (a) and (c), respectively.

Table 1 Comparisons of GSH-Pd in this study with other metal-based nanozymes

Enzyme	Substrate	K_m (mM)	$\upsilon_{max} \times 10^{-8}$ (Ms^{-1})
GSH-Pd3.5 (20 °C)	TMB	0.08	22.4
	H_2O_2	137	24.6
GSH-Pd2.6 (20 °C)	TMB	0.068	31.5
	H_2O_2	156	40.8
GSH-Pd1.4 (20 °C)	TMB	0.045	9.1
	H_2O_2	254	20.8
GSH-Pd2.6-Ag^+ [a] (20 °C)	TMB	0.106	20.9
	H_2O_2	190	32.6
GSH-Pd2.6-Hg^{2+} [b] (20 °C)	TMB	0.092	41.0
	H_2O_2	144	54.2
Pd nanostructures (room temperature)[27]	TMB	0.165	201
	H_2O_2	1064	443
GSH-Pt3.3 (20 °C)[35]	TMB	0.03	66.7
	H_2O_2	88.7	92.4
BSA-Pt2.0 (25 °C)[34]	TMB	0.119	21.0
	H_2O_2	41.8	16.7
Cu nanoclusters (30 °C)[45]	TMB	0.648	5.96
	H_2O_2	29.16	4.22
Au nanoclusters (40 °C)[46]	TMB	0.00253	6.23
	H_2O_2	25.3	7.21
Fe_3O_4 nanoparticles (40 °C)[44]	TMB	0.098	3.44
	H_2O_2	154	9.78
Co_3O_4 nanocubes (25 °C)[47]	TMB	0.037	6.27
	H_2O_2	140.07	12.1

[a] $[Ag^+]$ = 100 nM. [b] $[Hg^{2+}]$ = 1 μM.

signal (<3%). However, the A_{652} signal is intensified by 15% in the presence of 10-fold excess of Hg^{2+}. Therefore, we employed 1 μM EDTA into this sensing system. Consequently, addition of low concentration of EDTA can mask the interference of Hg^{2+}, while it shows little effect on the signal generated by Ag^+ (Fig. 4c). The LOD is calculated to be 1.27 nM with 1 μM EDTA added, and 1.23 nM upon addition of 500 nM Hg^{2+} and 1 μM EDTA (Fig. S9 and S10†). Therefore, it is demonstrated that GSH-Pd nanozyme possesses high feasibility for Ag^+ sensing in aqueous solution.

The mechanism of the Ag^+-induced inhibition of peroxidase mimicking activity was further investigated by XPS, TEM as well as enzyme kinetics. After adding equivalent molar Ag^+ into GSH-Pd2.6, the binding energy of Pd^0 shifted from 334.6 to 334.9 eV, which could be attributed to aurophilic attraction between d^{10} shells of Pd^0 and Ag^+ (Fig. 5a). The $Pd^0 \rightarrow Ag^+$ donor–acceptor bond is susceptible to reduce the electron density of Pd^0 and to cause an observed shift of the binding energy. According to kinetic studies, the affinities toward both TMB and H_2O_2 decrease in the presence of Ag^+ (listed Table 1). According to the TEM image, GSH-Pd2.6 tends to aggregate upon addition of equivalent molar of Ag^+ (Fig. 5b). It is suggested that Ag^+ can interact with Pd^0 species from different GSH-Pd, resulting in the observed aggregation of Pd nanoparticles. The apparent decrease of the GSH-Pd peroxidase-like activity should attribute to the Ag^+-induced reduction of Pd^0 electron density as well as the Ag^+-induced aggregation of GSH-Pd. In contrast, a slight shift to lower binding energy is monitored for Pd^0 species in the presence of Hg^{2+}. Addition of Hg^{2+} (10-fold concentration excess) causes an increase of the affinity toward H_2O_2 while a decrease of the affinity toward TMB. Although aggregation is also detected for GSH-Pd2.6

 This journal is © The Royal Society of Chemistry 2015

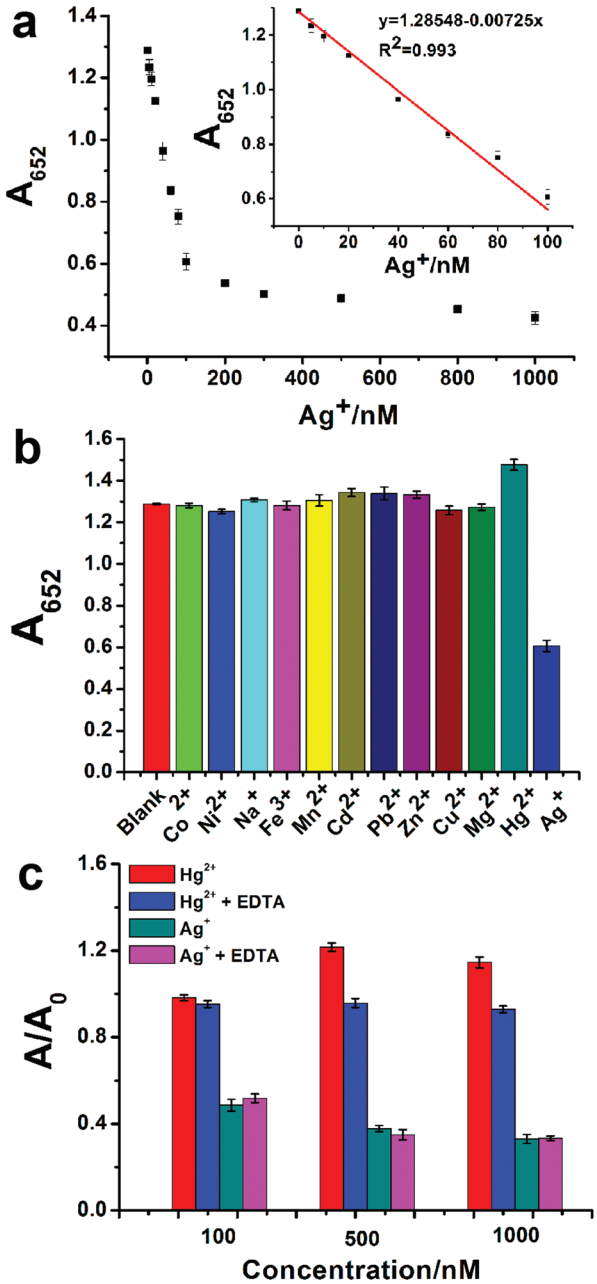

Fig. 4 (a) Plots of the A_{652} with the concentration of Ag^+, and the inset is the corresponding calibration curve. (b) The A_{652} in the TMB–H_2O_2 reaction catalyzed by GSH-Pd2.6 in the presence of 0.1 μM Ag^+, 1 μM metal ions including Na^+, Mg^{2+}, Cu^{2+}, Pb^{2+}, Cd^{2+}, Zn^{2+}, Ni^{2+}, Mn^{2+}, Fe^{3+}, Co^{2+} and Hg^{2+}, respectively. (c) Effect of 1 μM EDTA on the output signal generated by GSH-Pd2.6 in the presence of Ag^+ and Hg^{2+} respectively; The A_0 and A represent the A_{652} produced by GSH-Pd2.6 and GSH-Pd2.6-ion, respectively. The reaction system contains 0.125 mM TMB, 125 mM H_2O_2 and 900 nM Pd. The A_{652} is collected at 10 min after initiation.

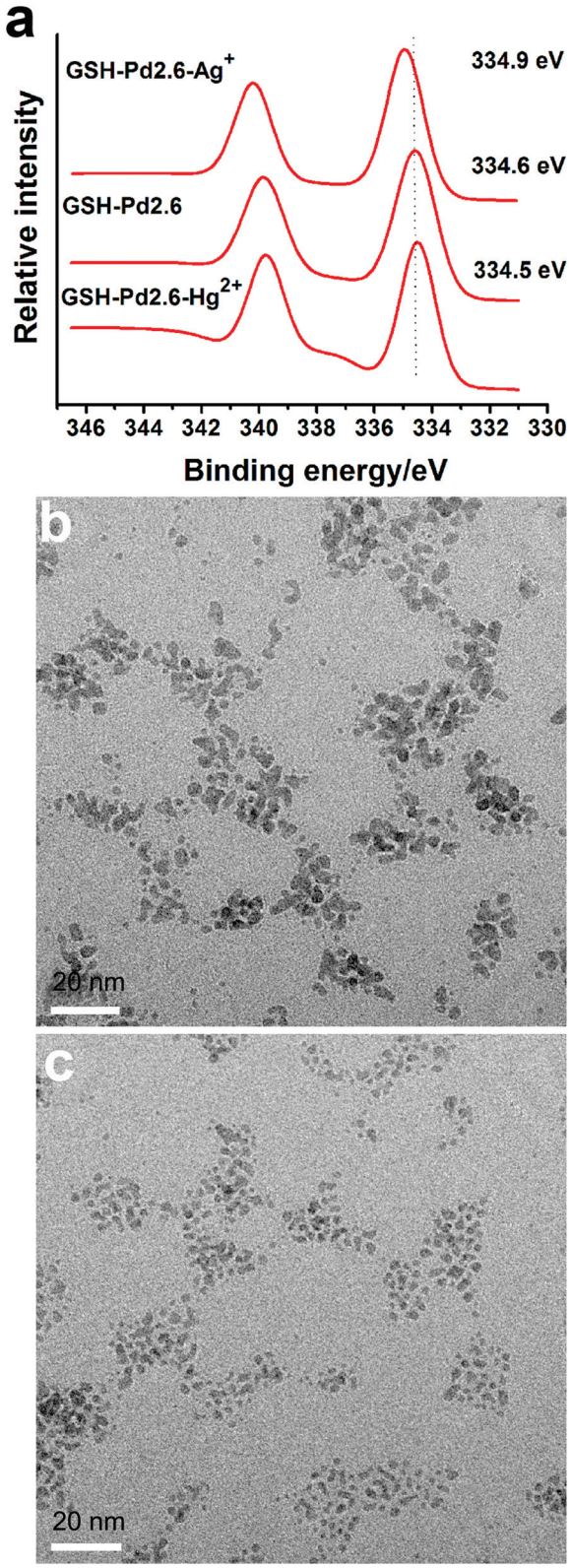

Fig. 5 (a) Pd 3d XPS spectra of GSH-Pd2.6 incubated with equivalent molar of Ag^+ and Hg^{2+}, respectively. TEM image of GSH-Pd2.6 upon addition of equivalent molar of Ag^+ (b) and Hg^{2+} (c).

Table 2 Comparisons of different Ag^+-sensing platforms

Method	System	LOD/ nM
Electrochemistry[50]	C-rich DNA-modified electrode	10
Electrochemistry[51]	Fe_3O_4@Au nanoparticles	59
Electrochemistry[52]	Alkanethiol-carbon nanotube-oligonucleotide electrodes	1.5
Fluorescence[53]	CH_3CN-MOPS	97
Fluorescence[54]	FAM-ssDNA/GO	50
Fluorescence[12]	DNA-Ag nanoclusters	10
Fluorescence[55]	CdS quantum dots	68
Colorimetry[56]	G-quadruplex-capped gold nanoparticles	7
Colorimetry[57]	G-quadruplex-hemin	64
Colorimetry (this work)	GSH-Pd2.6	1.2

(Fig. 5c), the v_{max} value shows that Hg^{2+} facilitates the peroxidase-like activities of GSH-Pd. Different metallophilic interactions have been reported to exhibit distinct effects on the peroxidase-like activity of metal nanoparticles. For example, Hg^{2+} significantly enhances the peroxidase-like activity of Au nanoparticles while it inhibits the related activity of Pt nanoparticles.[48,49] Therefore, it is reasonable to conclude that Hg^{2+} and Ag^+ show the opposite influence on the peroxidase-like activity of Pd-based nanozyme.

To validate the sensing application of GSH-Pd in real samples, spiked-recovery experiments were carried out in the lake water upon addition of 1 μM EDTA. The recovery rates are calculated as 121%, 111% and 92% for 20, 50 and 80 nM spiked Ag^+, respectively (Table S1†). It is suggested that the concentration of Ag^+ detected by ICP-MS is lower than the concentration determined by the colorimetric method proposed in this study. Compared with other detection methods listed in Table 2, GSH-Pd nanozyme can be recognized as a promising candidate for quantitative determination of Ag^+ in drinking water, owing to several advantages such as low LOD, low material and energy consumption, as well as green synthesis.

Further, we tested the potential application of this sensing system on the detection of Ag nanoparticles. UV-vis spectra of as-prepared citrate-capped Ag nanoparticles with the size distribution of 5–20 nm, exhibit a maximum absorption peak at 412 nm (Fig. S13 and S14†). Upon addition of H_2O_2, the absorption band gradually decreases within 30 min, suggesting the H_2O_2-mediated oxidation of Ag nanoparticles. In the TMB–H_2O_2 reaction catalyzed by GSH-Pd2.6, the A_{652} signal gradually decreases with the concentration of Ag nanoparticles (Fig. S15†). A good linear relationship can be obtained in the concentration range of 10–100 nM, with the LOD of 6.1 nM. It is demonstrated that GSH-Pd nanozyme can be potentially utilized for colorimetric detection of Ag nanoparticles.

4. Conclusion

Pd nanoparticles are facilely synthesized by using GSH as the nucleation template, showing highly peroxidase-like activity. The molar ratio of [Na_2PdCl_4]/[GSH] significantly affects the physicochemical properties of GSH-Pd including particle sizes, surface charge states and enzymatic activities. The most efficient Pd nanozyme consisting of approximately 57% Pd^0 species with an average diameter of 2.6 nm, exhibit the K_m value of 0.068 mM toward TMB and 156 mM toward H_2O_2. Ag^+ selectively binds to Pd^0 species through metallophilic interactions and inhibits the peroxidase-like activity of Pd nanoparticles. GSH-Pd is employed to explore colorimetric detection of Ag^+ in aqueous solution, resulting in the LOD of 1.2 nM. This developed sensing system is potentially applicable for quantitative detection of Ag^+ in drinking water samples as well as Ag nanoparticles in the aqueous solution.

Acknowledgements

This work was supported by the National Natural Science Foundation of China (21206107, 31200753).

References

1 C. Z. Lai, M. A. Fierke, R. C. da Costa, J. A. Gladysz, A. Stein and P. Bühlmann, *Anal. Chem.*, 2010, **82**, 7634–7640.
2 H. T. Ratte, *Environ. Toxicol. Chem.*, 1999, **18**, 89–108.
3 S. Y. Liau, D. C. Read, W. J. Pugh, J. R. Furr and A. D. Russull, *Lett. Appl. Microbiol.*, 1997, **25**, 279–283.
4 T. N. Wells, P. Scully, G. Paravicini, A. E. Proudfoot and M. A. Payton, *Biochemistry*, 1995, **34**, 7896–7903.
5 J. F. Zhang, Y. Zhou, J. Yoon and J. S. Kim, *Chem. Soc. Rev.*, 2011, **40**, 3416–3429.
6 X. Yang and E. K. Wang, *Anal. Chem.*, 2011, **83**, 5005–5011.
7 Y. Wen, F. Xing, S. He, S. Song, L. Wang, Y. Long, D. Li and C. Fan, *Chem. Commun.*, 2010, **46**, 2596–2598.
8 K. Mao, Z. T. Wu, Y. R. Chen, X. D. Zhou, A. G. Shen and J. M. Hu, *Talanta*, 2015, **132**, 658–663.
9 J. Lee, J. Park, H. H. Lee, H. Park, H. I. Kim and W. J. Kim, *Biosens. Bioelectron.*, 2015, **68**, 642–647.
10 Q. S. Pu, Q. Y. Sun, Z. Hu and Z. X. Su, *Analyst*, 1998, **123**, 239–243.
11 M. Hosoba, K. Oshita, R. K. Katarina, T. Takayanagi, M. Oshima and S. Motomizu, *Anal. Chim. Acta*, 2009, **639**, 51–56.
12 X. B. Zhang, Z. X. Han, Z. H. Fang, G. L. Shen and R. Q. Yu, *Anal. Chim. Acta*, 2006, **562**, 210–215.
13 Y. M. Sung and S. P. Wu, *Sens. Actuators, B*, 2014, **197**, 172–176.
14 J. L. Zhang, X. Wang, Y. Fu, Y. Han, J. Y. Cheng, Y. Q. Zhang and W. Li, *Langmuir*, 2013, **29**, 14345–14350.
15 R. Coppage, J. M. Slocik, B. D. Briggs, A. I. Frenkel, H. Heinz, R. R. Naik and M. R. Knecht, *J. Am. Chem. Soc.*, 2011, **133**, 12346–12349.
16 B. Lim, M. J. Jiang, J. Tao, P. H. C. Camargo, Y. M. Zhu and Y. N. Xia, *Adv. Funct. Mater.*, 2009, **19**, 189–200.

 This journal is © The Royal Society of Chemistry 2015

17 Y. Mei, Y. Lu, F. Polzer, M. Ballauff and M. Drechsler, *Chem. Mater.*, 2007, **19**, 1062–1069.
18 K. Esumi, R. Isono and T. Yoshimura, *Langmuir*, 2004, **20**, 237–243.
19 R. Bhandari and M. R. Knecht, *ACS Catal.*, 2011, **1**, 89–98.
20 S. Behrens, A. Heyman, R. Maul, S. Essig, S. Steigerwald, A. Quintilla, W. Wenzel, J. Burck, O. Dgany and O. Shoseyov, *Adv. Mater.*, 2009, **21**, 3515–3519.
21 K. G. Qu, L. Wu, J. S. Ren and X. G. Qu, *ACS Appl. Mater. Interfaces*, 2012, **4**, 5001–5009.
22 K. Zhang, X. N. Hu, J. B. Liu, J. J. Yin, S. A. Hou, T. Wen, W. W. He, Y. L. Ji, Y. T. Guo, Q. Wang and X. C. Wu, *Langmuir*, 2011, **27**, 2796–2803.
23 X. M. Chen, B. Y. Su, Z. X. Cai, X. Chen and M. Oyama, *Sens. Actuators, B*, 2014, **201**, 286–292.
24 X. J. Zheng, Q. Zhu, H. Q. Song, X. R. Zhao, T. Yi, H. L. Chen and X. G. Chen, *ACS Appl. Mater. Interfaces*, 2015, **7**, 3480–3491.
25 W. J. Shi, H. Fan, S. Y. Ai and L. S. Zhu, *RSC Adv.*, 2015, **5**, 32183–32190.
26 J. M. Lan, W. M. Xu, Q. P. Wan, X. Zhang, J. Lin, J. H. Chen and J. Z. Chen, *Anal. Chim. Acta*, 2014, **825**, 63–68.
27 Z. Q. Gao, L. Hou, M. D. Xu and D. P. Tang, *Sci. Rep.*, 2014, **4**, 3966.
28 D. H. Tian, Z. S. Qian, Y. S. Xia and C. Q. Zhu, *Langmuir*, 2012, **28**, 3945–3951.
29 C. J. Yu, T. H. Chen, J. Y. Jiang and W. L. Tseng, *Nanoscale*, 2014, **6**, 9618–9624.
30 J. P. Xie, Y. G. Zheng and J. Y. Ying, *Chem. Commun.*, 2010, **46**, 961–963.
31 L. H. Doerrer, *Dalton Trans.*, 2010, **39**, 3543–3553.
32 G. W. Wu, S. B. He, H. P. Peng, H. H. Deng, A. L. Liu, X. H. Lin, X. H. Xia and W. Chen, *Anal. Chem.*, 2014, **86**, 10955–10960.
33 Y. Fu, X. Y. Zhao, J. L. Zhang and W. Li, *J. Phys. Chem. C*, 2014, **118**, 18116–18125.
34 W. Li, B. Chen, H. X. Zhang, Y. H. Sun, J. Wang, J. L. Zhang and Y. Fu, *Biosens. Bioelectron.*, 2015, **66**, 251–258.
35 W. Li, H. X. Zhang, J. L. Zhang and Y. Fu, *Anal. Methods*, 2015, **7**, 4464–4471.
36 A. A. Sousa, J. T. Morgan, P. H. Brown, A. Adams, M. P. S. Jayasekara, G. F. Zhang, C. J. Ackerson, M. J. Kruhlak and R. D. Leapman, *Small*, 2012, **8**, 2277–2286.
37 S. Sharma, B. Kim and D. Lee, *Langmuir*, 2012, **28**, 15958–15965.
38 X. Yuan, Y. Q. Tay, X. Y. Dou, Z. T. Luo, D. T. Leong and J. P. Xie, *Anal. Chem.*, 2013, **85**, 1913–1919.
39 Z. K. Wu, J. Chen and R. C. Jin, *Adv. Funct. Mater.*, 2011, **21**, 177–183.
40 C. V. Pagba, S. M. Lane and S. Wachsmann-Hogiu, *J. Raman Spectrosc.*, 2010, **41**, 241–247.
41 M. R. Knecht, M. G. Weir, V. S. Myers, W. D. Pyrz, H. C. Ye, V. Petkov, D. J. Buttrey, A. I. Frenkel and R. M. Crooks, *Chem. Mater.*, 2008, **20**, 5218–5228.
42 A. Desireddy, B. E. Conn, J. S. Guo, B. Yoon, R. N. Barnett, B. M. Monahan, K. Kirschbaum, W. P. Griffith, R. L. Whetten, U. Landman and T. P. Bigioni, *Nature*, 2013, **501**, 399–402.
43 H. Wei, Z. D. Wang, L. M. Yang, S. L. Tian, C. J. Hou and Y. Lu, *Analyst*, 2010, **135**, 1406–1410.
44 L. Z. Gao, J. Zhuang, L. Nie, J. B. Zhang, Y. Zhang, N. Gu, T. H. Wang, J. Feng, D. L. Yang, S. Perrett and X. Yan, *Nat. Nanotechnol.*, 2007, **2**, 577–583.
45 L. Z. Hu, Y. L. Yuan, L. Zhang, J. M. Zhao, S. Majeed and G. B. Xu, *Anal. Chim. Acta*, 2013, **762**, 83–86.
46 X. X. Wang, Q. Wu, Z. Shan and Q. M. Huang, *Biosens. Bioelectron.*, 2011, **26**, 3614–3619.
47 J. S. Mu, Y. Wang, M. Zhao and L. Zhang, *Chem. Commun.*, 2012, **48**, 2540–2542.
48 Y. J. Long, Y. F. Li, Y. Liu, J. J. Zheng, J. Tang and C. Z. Huang, *Chem. Commun.*, 2011, **47**, 11939–11941.
49 G. W. Wu, S. B. He, H. P. Peng, H. H. Deng, A. L. Liu, X. H. Lin, X. H. Xia and W. Chen, *Anal. Chem.*, 2014, **86**, 10955–10960.
50 Z. Z. Lin, X. H. Li and H. B. Kraatz, *Anal. Chem.*, 2011, **83**, 6896–6901.
51 H. C. Yang, X. X. Liu, R. H. Fei and Y. G. Hu, *Talanta*, 2013, **116**, 548–553.
52 Z. P. Zhang and J. Yan, *Sens. Actuators, B*, 2014, **202**, 1058–1064.
53 Y. L. Lv, L. L. Zhu, H. Liu, Y. S. Wu, Z. L. Chen, H. B. Fu and Z. Y. Tian, *Anal. Chim. Acta*, 2014, **839**, 74–82.
54 X. Chen, Y. R. Chen, X. D. Zhou and J. M. Hu, *Talanta*, 2013, **107**, 277–283.
55 T. Khantaw, C. Boonmee, T. Tuntulani and W. Ngeontae, *Talanta*, 2013, **115**, 849–856.
56 G. M. Liu, Q. X. Zhang, Y. Qian, S. P. Yu and F. Li, *Anal. Methods*, 2013, **5**, 648–652.
57 X. H. Zhou, D. M. Kong and X. H, *Anal. Chem.*, 2010, **82**, 789–793.

This journal is © The Royal Society of Chemistry 2015